Submitted to

International Europhysics Conference on High Energy Physics, EPS03, July 17-23, 2003, Aachen
(Abstract **101** Parallel Session **13**)

XXI International Symposium on Lepton and Photon Interactions, LP03, August 11-16, 2003, Fermilab

www-h1.desy.de/h1/www/publications/conf/conf_list.html

Searches for Squark Production in R-Parity Violating Supersymmetry at HERA

H1 Collaboration

Abstract

A search for squarks in R-parity violating supersymmetry has been performed in $e^{\pm}p$ collisions at HERA using the H1 detector. The data taken at a centre of mass energy of $319\,\mathrm{GeV}$ correspond to an integrated luminosity of $63.5\,\mathrm{pb}^{-1}$ for $e^{+}p$ collisions and $13.5\,\mathrm{pb}^{-1}$ for $e^{-}p$ collisions. The resonant production of squarks via a Yukawa coupling λ' has been considered and various decay topologies of squarks have been investigated. No significant deviation from the Standard Model has been found. The results are interpreted in terms of exclusion limits within the Minimal Supersymmetric Standard Model (MSSM) and the minimal Supergravity Model. All flavours of squarks have been searched for. Squark masses below $275\,\mathrm{GeV}$ are excluded at $95\,\%$ confidence level in a large part of the parameter space for a Yukawa coupling of electromagnetic strength.

1 Introduction

The ep collider HERA is ideally suited to look for new particles coupling to an electron-quark pair. In supersymmetric (SUSY) models with R-parity violation ($\not{R}_p$), squarks can couple to electrons (or positrons) and quarks via a Yukawa coupling λ'. At HERA squarks could be produced resonantly via the fusion of the incoming electron (or positron) with an energy of $27.6\,\mathrm{GeV}$ and a quark from the incoming proton of energy $920\,\mathrm{GeV}$. Squark masses up to the centre of mass energy $\sqrt{s} = 319\,\mathrm{GeV}$ are kinematically accessible.

The data used in this analysis were taken from 1998 to 2000 when HERA was operating with both an initial electron and an initial positron beam. The data sets correspond to an integrated luminosity of $63.5\,\mathrm{pb}^{-1}$ for e^+p collisions and $13.5\,\mathrm{pb}^{-1}$ for e^-p collisions. This extends the searches for squark production in e^+p and e^-p collisions previously performed by H1 [1, 2] at lower centre of mass energy ($\sqrt{s} = 301\,\mathrm{GeV}$) and with lower statistics ($37\,\mathrm{pb}^{-1}$ for e^+p and $425\,\mathrm{nb}^{-1}$ for e^-p). The analyses of e^+p and e^-p collisions allow for tests of different Yukawa couplings and different squark types; with the two data sets all flavours of squarks can be searched for.

2 Phenomenology

The most general supersymmetric theory that is renormalizable and gauge invariant with respect to the Standard Model (SM) gauge group allows for couplings between two ordinary fermions and a squark or a slepton. In such theories the R-parity, which is defined as $R_p = (-1)^{3B+L+2S}$, where S denotes the spin, B the baryon number and L the lepton number of the particles, is not conserved. The Yukawa couplings between a lepton-quark pair and a squark are described in the superpotential by the R_p-violating terms $\lambda'_{ijk} L_i Q_j \bar{D}_k$, where i, j, k are family indices. The corresponding part of the Lagrangian is given by:

$$\begin{aligned} \mathcal{L}_{L_i Q_j \bar{D}_k} &= \lambda'_{ijk} \Big[-\tilde{e}^i_L u^j_L \bar{d}^k_R - e^i_L \tilde{u}^j_L \bar{d}^k_R - (\bar{e}^i_L)^c u^j_L \tilde{d}^{k*}_R \\ &\quad + \tilde{\nu}^i_L d^j_L \bar{d}^k_R + \nu_L \tilde{d}^j_L \bar{d}^k_R + (\bar{\nu}^i_L)^c d^j_L \tilde{d}^{k*}_R \Big] + \text{c.c.} \end{aligned} \tag{1}$$

where the superscripts c denote the charge conjugate spinors and the $*$ the complex conjugate of scalar fields. The coupling λ'_{1jk} allows for resonant production of squarks at HERA through eq fusion [3]. The search presented here has been performed under the assumption that one of the λ'_{1jk} dominates. In table 1 all possible production processes for ep reactions are listed. With an initial e^+ beam HERA is most sensitive to couplings λ'_{1j1}, where mainly $\tilde{u}^j_L$ squarks (i.e. $\tilde{u}_L, \tilde{c}_L, \tilde{t}_L$) are being produced, whereas with an initial e^- beam HERA is most sensitive to couplings λ'_{11k} and could mainly produce $\tilde{d}^k_R$ squarks (i.e. $\tilde{d}_R, \tilde{s}_R, \tilde{b}_R$). The production cross-section in e^+p collisions is proportional to $\lambda'^2_{1j1} \cdot d(x)$ where $d(x)$ is the probability to find a d quark in the proton with a momentum fraction $x = M^2_{\tilde{q}}/s$ and $M_{\tilde{q}}$ denotes the squark mass. Similarly, the production cross-section in e^-p collisions scales as $\lambda'^2_{11k} \cdot u(x)$ with $u(x)$ being the probability to find a u quark in the proton with a momentum fraction $x = M^2_{\tilde{q}}/s$. Thus, the squark production cross section in e^-p running is potentially larger compared to e^+p running.

λ'_{1jk}	e^+p		e^-p	
111	$e^+ + d \to \tilde{u}_L$	$e^+ + \overline{u} \to \overline{\tilde{d}_R}$	$e^- + u \to \tilde{d}_R$	$e^- + \overline{d} \to \overline{\tilde{u}_L}$
112	$e^+ + s \to \tilde{u}_L$	$e^+ + \overline{u} \to \overline{\tilde{s}_R}$	$e^- + u \to \tilde{s}_R$	$e^- + \overline{s} \to \overline{\tilde{u}_L}$
113	$e^+ + b \to \tilde{u}_L$	$e^+ + \overline{u} \to \overline{\tilde{b}_R}$	$e^- + u \to \tilde{b}_R$	$e^- + \overline{b} \to \overline{\tilde{u}_L}$
121	$e^+ + d \to \tilde{c}_L$	$e^+ + \overline{c} \to \overline{\tilde{d}_R}$	$e^- + c \to \tilde{d}_R$	$e^- + \overline{d} \to \overline{\tilde{c}_L}$
122	$e^+ + s \to \tilde{c}_L$	$e^+ + \overline{c} \to \overline{\tilde{s}_R}$	$e^- + c \to \tilde{s}_R$	$e^- + \overline{s} \to \overline{\tilde{c}_L}$
123	$e^+ + b \to \tilde{c}_L$	$e^+ + \overline{c} \to \overline{\tilde{b}_R}$	$e^- + c \to \tilde{b}_R$	$e^- + \overline{b} \to \overline{\tilde{c}_L}$
131	$e^+ + d \to \tilde{t}_L$	$e^+ + \overline{t} \to \overline{\tilde{d}_R}$	$e^- + t \to \tilde{d}_R$	$e^- + \overline{d} \to \overline{\tilde{t}_L}$
132	$e^+ + s \to \tilde{t}_L$	$e^+ + \overline{t} \to \overline{\tilde{s}_R}$	$e^- + t \to \tilde{s}_R$	$e^- + \overline{s} \to \overline{\tilde{t}_L}$
133	$e^+ + b \to \tilde{t}_L$	$e^+ + \overline{t} \to \overline{\tilde{b}_R}$	$e^- + t \to \tilde{b}_R$	$e^- + \overline{b} \to \overline{\tilde{t}_L}$

Table 1: Squark production processes in $e^{\pm}p$ collisions.

In R-parity violating supersymmetry squarks decay either via their Yukawa coupling λ' into SM fermions, or via their usual gauge couplings into a gluino $\tilde{g}$, a neutralino χ_i^0 $(i = 1, 4)$ or a chargino $\chi_i^{\pm}$ $(i = 1, 2)$. Because R_p is violated the Lightest Supersymmetric Particle (LSP) is not stable, but decays via a virtual squark or slepton into a quark, an antiquark and a lepton [3]. In this analysis the LSP is assumed to be a neutralino, chargino or gluino.

If both production and decay occur via a λ'_{1jk} coupling, the squarks will have the same signature as scalar leptoquarks (LQ) [4]. As can be seen from equation (1), the $\tilde{d}_R^k$ produced in e^-p collisions can decay either into $e^- + u^j$ or $\nu_e + d^j$, while the $\tilde{u}_L^j$ which is produced in e^+p collisions decays into $e^+ + d^k$ only. The final state consists of a jet and either an electron (or positron) with high transverse momentum (p_T) or missing p_T leading to signatures similar to SM neutral current (NC) and charged current (CC) Deep-Inelastic Scattering (DIS).

When the squark undergoes a gauge decay into a χ^0, a χ^+ or a $\tilde{g}$ the final state will depend on their subsequent decays. Neutralinos χ_i^0 with $i > 1$ as well as charginos (gluinos) usually undergo gauge decays into a lighter χ and two SM fermions (two quarks), through a (real or virtual) gauge boson or sfermion (squark). The decay chain ends with the $\not{R}_p$ decay of one sparticle, usually that of the LSP.

$\not{R}_p$ decays of χ's or gluinos are mainly relevant for the lightest states. Neutralinos can undergo the $\not{R}_p$ decays $\chi^0 \to e^{\pm}q\bar{q}'$ or $\chi^0 \to \nu q\bar{q}$, the former (latter) being more frequent if the χ^0 is dominated by its photino (zino) component. Gluinos can undergo the same $\not{R}_p$ decays. When a χ^0 or a $\tilde{g}$ decays via $\not{R}_p$ into a charged lepton, both the 'right' and the 'wrong' charge lepton (with respect to the incident beam) are equally probable, the latter case leading to largely background free striking signatures for lepton number violation. In contrast, the only possible $\not{R}_p$ decays for charginos are $\chi^+ \to \bar{\nu}u^k\bar{d}^j$ and $\chi^+ \to e^+d^k\bar{d}^j$.

The decay chains of $\tilde{u}_L^j$ and $\tilde{d}_R^k$ analysed in this paper are classified into seven distinguishable event topologies as described in table 2. This classification relies on the number of charged leptons and/or jets in the final state, and on the presence of missing energy. Channels labelled with $\boldsymbol{eLQ}$ and $\boldsymbol{\nu LQ}$ are the "leptoquark-like" decay modes of the squark, proceeding directly via $\not{R}_p$, while the remaining channels cover the gauge decays of the squark and are characterised by multijet (MJ) final states. Channels labelled with $\boldsymbol{e^+MJ}$, $\boldsymbol{e^-MJ}$ and $\boldsymbol{\nu MJ}$ involve one or two SUSY fermions (χ or $\tilde{g}$) denoted by X and Y in table 2. Channels $\boldsymbol{e\ell MJ}$ and $\boldsymbol{\nu\ell MJ}$ necessarily involve two SUSY fermions. Decay patterns involving more than two χ or $\tilde{g}$ are kinematically suppressed and therefore not explicitly searched for. Decays of χ's into Higgs boson are taken into account, when the Higgs decays into hadrons. The contribution of these decays is however very small. In the mass range considered here the sum of branching ratios of the considered channels is very close to 1 for basically all SUSY scenarios [1].

Cases where the χ_1^0 has such a small decay width that it leads to displaced vertices have not been considered, since the region of parameter space which would allow a χ^0 to escape detection for a finite value of the $\not{R}_p$ coupling is now very strongly constrained by the searches for charginos carried out at LEP [5].

3 The H1 detector

The detector components of the H1 experiment most relevant for this analysis are briefly described in the following. A detailed description can be found in [6]. The main components of the tracking system are central drift and proportional chambers in the polar angle [1] range $25° \leq \theta \leq 155°$, a forward track detector ($7° \leq \theta \leq 25°$) and a backward drift chamber. The tracking system is surrounded by a finely segmented liquid argon (LAr) calorimeter [7] covering the polar angular range $4° \leq \theta \leq 154°$ with energy resolution of $\sigma(E)/E \simeq 12\%/\sqrt{E/\mathrm{GeV}} \oplus 1\%$ for electrons and $\sigma(E)/E \simeq 50\%/\sqrt{E/\mathrm{GeV}} \oplus 2\%$ for hadrons, obtained in test beam measurements [8]. For the acquisition of events we rely on the LAr trigger system [7] whose efficiency is close to 100% for the transverse momenta (p_T) considered here. The tracking chambers and calorimeters are surrounded by a superconducting solenoid and an iron yoke instrumented with streamer tubes which is used to measure leakage of hadronic showers and to identify muons. The luminosity is determined from the rate of Bethe-Heitler $ep \rightarrow ep\gamma$ bremsstrahlung events measured in a luminosity monitor.

4 Monte Carlo Event Generation

Complete Monte Carlo simulations of the H1 detector response have been performed for various Monte Carlo samples in order to determine the amount of SM background in the selection and to determine the signal detection efficiencies. For each possible SM background source a sample of Monte Carlo events was used corresponding to a luminosity of more than 10 times that of the data.

The determination of the contribution of NC DIS processes is performed using two Monte Carlo Samples which employ different models of QCD radiation. The first was produced with the DJANGO [9] event generator which includes QED first order radiative corrections. QCD radiation is implemented using ARIADNE [10] based on the Colour Dipole Model [11]. This sample is chosen to estimate the NC DIS contribution in the $\boldsymbol{eLQ}$ channel. The second sample

[1] The polar angle θ is measured with respect to the proton beam direction.

Channel	Decay processes	Signature
$\boldsymbol{eLQ}$	$\tilde{q} \xrightarrow{\lambda'} e \quad q$	high p_T e + 1 jet
$\boldsymbol{\nu LQ}$	$\tilde{d}^k_R \xrightarrow{\lambda'} \nu_e \quad d$	missing p_T + 1 jet
$\boldsymbol{e^+MJ}$	$\tilde{q} \longrightarrow q \quad X$ $\overset{\lambda'}{\hookrightarrow} e^+\bar{q}q$ $\tilde{q} \longrightarrow q \quad X$ $\hookrightarrow q\bar{q} \quad Y$ $\overset{\lambda'}{\hookrightarrow} e^+\bar{q}q$	e^+ + multiple jets
$\boldsymbol{e^-MJ}$	$\tilde{q} \longrightarrow q \quad \chi^0_i, \tilde{g}$ $\overset{\lambda'}{\hookrightarrow} e^-\bar{q}q$ $\tilde{q} \longrightarrow q \quad X$ $\hookrightarrow q\bar{q} \quad Y$ $\overset{\lambda'}{\hookrightarrow} e^-\bar{q}q$	e^- + multiple jets
$\boldsymbol{\nu MJ}$	$\tilde{q} \longrightarrow q \quad X$ $\overset{\lambda'}{\hookrightarrow} \nu\bar{q}q$ $\tilde{q} \longrightarrow q \quad X$ $\hookrightarrow q\bar{q} \; Y$ $\overset{\lambda'}{\hookrightarrow} \nu\bar{q}q'$	missing p_T + multiple jets
$\boldsymbol{e\ell MJ}$	$\tilde{q} \longrightarrow q \quad X$ $\hookrightarrow \ell\nu_\ell \quad Y$ $\overset{\lambda'}{\hookrightarrow} e^\pm\bar{q}q$ $\tilde{q} \longrightarrow q \quad X$ $\hookrightarrow \ell^+\ell^- \quad Y$ $\overset{\lambda'}{\hookrightarrow} e^\pm\bar{q}q$ $\tilde{q} \longrightarrow q \quad X$ $\hookrightarrow e^+e^- \quad Y$ $\overset{\lambda'}{\hookrightarrow} \nu\bar{q}q$	e + ℓ (e or μ) + multiple jets
$\boldsymbol{\nu\ell MJ}$	$\tilde{q} \longrightarrow q \quad X$ $\hookrightarrow \ell\nu_\ell \quad Y$ $\overset{\lambda'}{\hookrightarrow} \nu\bar{q}q$ $\tilde{q} \longrightarrow q \quad X$ $\hookrightarrow \mu^+\mu^- \quad Y$ $\overset{\lambda'}{\hookrightarrow} \nu\bar{q}q$	ℓ (e or μ) + missing p_T + multiple jets

Table 2: Squark decay channels in $\not{R}_p$ SUSY classified by distinguishable event topologies. X and Y denote a neutralino, a chargino or a gluino. Quarks are generically denoted by q, except for the $\boldsymbol{\nu LQ}$ channel which involves specific (s)quark flavours. The final states corresponding to $\ell = \tau$ for the $\boldsymbol{e\ell MJ}$ and $\boldsymbol{\nu\ell MJ}$ channels are not explicitly looked for in this analysis.

was generated with the program RAPGAP [12], in which QED first order radiative corrections are implemented as described above. RAPGAP includes leading order QCD matrix elements and higher order radiative corrections are modelled by leading-log parton showers [13]. This sample is used to determine NC DIS background in the final states with electron or positron and multiple jets, as RAPGAP better describes this particular phase space domain [14]. For both samples the parton densities in the proton are taken from the CTEQ5D [15] parametrization. Hadronisation is performed in the Lund string fragmentation scheme using JETSET [16]. The modelling of the CC DIS process is performed using the DJANGO program with CTEQ5D structure functions. Direct and resolved photoproduction processes (γp) of light and heavy flavours including prompt photon production are generated with the PYTHIA [17] event generator which relies on first order matrix elements and uses leading-log parton showers and string fragmentation [16]. The SM prediction for $ep \to eW^{\pm}X$ and $ep \to eZX$ is calculated with EPVEC [18].

For the determination of the signal detection efficiencies in the $\boldsymbol{eLQ}$ and $\boldsymbol{\nu LQ}$ channels, we make use of the LEGO event generator [19]. LEGO takes into account initial QED radiation in the collinear approximation. For the squark decays involving gauginos (neutralinos, charginos, gluinos) we use the SUSYGEN [20] generator. In both LEGO and SUSYGEN, initial and final state parton showers are simulated following the DGLAP [13] evolution equations, and string fragmentation [16] is used for the non-perturbative part of the hadronisation. The parton densities are evaluated at the scale of the squark mass. This scale is also chosen for the maximum virtuality of parton showers initiated by a quark coming from the squark decay. Moreover, in the SUSYGEN generator, the parton showers modelling QCD radiation off quarks emerging from a χ or $\tilde{g}$ decay are started at a scale given by the mass of this sparticle.

To allow for a model independent interpretation of the results, the signal topologies given in table 2 were simulated for a wide range of masses of the SUSY particles. The squark mass was varied from $100\,\mathrm{GeV}$ to $290\,\mathrm{GeV}$ in steps of $25\,\mathrm{GeV}$. Gauge decays of squarks involving one or two SUSY fermions (χ or $\tilde{g}$) were simulated separately. For gauge decays of squarks into a χ^0, a χ^+ or a $\tilde{g}$ which directly decays via $\not{R}_p$ (i.e. processes corresponding to the first line of the $\boldsymbol{e^+MJ}$, $\boldsymbol{e^-MJ}$ and $\boldsymbol{\nu MJ}$ rows in table 2) the process $\tilde{q} \to q\chi_1^0$ was simulated for χ_1^0 masses ranging between $30\,\mathrm{GeV}$ and $270\,\mathrm{GeV}$. In order to study gauge decays involving two χ or $\tilde{g}$, the process $\tilde{q} \to q\chi_1^+ \to q\chi_1^0 f\bar{f}'$ was simulated for χ_1^+ masses ranging between $40\,\mathrm{GeV}$ and $\sim M_{\tilde{q}}$, and for χ_1^0 masses between $30\,\mathrm{GeV}$ and $\sim M_{\chi_1^+}$. Masses of the χ's were varied in steps of about $10\,\mathrm{GeV}$. These simulations allowed the determination of signal selection efficiencies as a function of the masses of the squark and of the involved χ or $\tilde{g}$ for essentially all allowed scenarios, since the grid size chosen for the simulated scenarios was small enough for a linear interpolation between them.

5 Event Selection

Background events not related to ep collisions are rejected by requiring that a primary interaction vertex be reconstructed with $\pm 35\,\mathrm{cm}$ of the nominal vertex position, by using filters based on the event topology and by requiring an event time which is consistent with the interaction time.

The following identification criteria are used to select events containing leptons, hard jets, or missing transverse energy: An **electron (or positron)** is identified by a shower shape analysis of energy deposits in the LAr calorimeter selecting isolated and compact electromagnetic clusters. A **muon** candidate is identified as a track measured in the central and/or forward tracking system, which has to match geometrically an energy deposit in the LAr calorimeter compatible with a minimum ionising particle, and/or a track in the instrumented iron and/or a track in the forward muon detector. **Hadronic jets** are reconstructed from energy deposits in the LAr calorimeter using a cone algorithm in the laboratory frame with a radius $\sqrt{\Delta\eta^2 + \Delta\phi^2} = 1$, where $\eta = -\ln\tan\frac{\theta}{2}$ is the pseudorapidity and ϕ denotes the azimuthal angle. **Missing transverse momentum** $p_{T,\mathrm{miss}}$ is obtained by summation of all energy deposits in the calorimeters.

For the further selection the following Lorentz invariant variables are important:

$$y_e = 1 - \frac{E_e(1-\cos\theta_e)}{2E_e^0}, \quad Q_e^2 = \frac{p_{T,e}^2}{1-y_e}, \quad x_e = \frac{Q_e^2}{y_e s}, \quad M_e = \sqrt{x_e s} \ .$$

They are determined using the measurement of the polar angle θ_e, the energy E_e and the transverse momentum $p_{T,e}$ of the highest p_T positron or electron found in the event. E_e^0 denotes the energy of the incident electron (or positron). In addition they can be calculated using the Jacquet-Blondel ansatz:

$$y_h = \frac{\sum(E-p_z)_h}{2E_e^0}, \quad Q_h^2 = \frac{p_{T,h}^2}{1-y_h}, \quad x_h = \frac{Q_h^2}{y_h s}, \quad M_h = \sqrt{x_h s} \ ,$$

where $p_{T,h}$ and $\sum(E-p_z)_h$ are calculated from the hadronic energy deposits in the LAr.

5.1 R-parity violating squark decays

The final states of squarks decaying in the channel $\boldsymbol{eLQ}$ and NC DIS reactions are identical. However, the distribution of the events in M_e and y_e is different. Squark decays via $\boldsymbol{eLQ}$ lead to a resonance peak in the M_e distribution. The resolution in M_e is between 3 and 6 GeV depending on the squark mass. Squarks produced in the s-channel decay isotropically in their rest frame leading to a flat $d\sigma/dy$ distribution. In contrast the $d\sigma/dy \propto y^{-2}$ distribution of NC DIS events is markedly different. These differences are used to enhance the SUSY signal over the DIS background by applying an optimised lower y_e-cut depending on the squark mass.

The selection criteria for the $\boldsymbol{eLQ}$ channel are the following:

- The total transverse momentum of the events must be balanced: $p_{T,\mathrm{miss}} < 15\,\mathrm{GeV}$.
- The reconstructed momentum loss in the direction of the incident electron/positron must be limited, such that $40 \leq \sum(E-p_z) \leq 70\,\mathrm{GeV}$ [2].
- An electron (or positron) must be found in the LAr with $p_{T,e} > 16\,\mathrm{GeV}$. For electrons (or positrons) in the central detector region ($\theta_e > 40°$) at least one charged track pointing to the electromagnetic cluster is required.

[2] Signal events lead to a peak at $\sum(E-p_z) = 2E_e^0 = 55\,\mathrm{GeV}$

H1 preliminary e^+p

Channel	data	SM prediction
eLQ	690	705.9 ± 51.3
e^-MJ	0	0.33 ± 0.15
e^+MJ	104	89.6 ± 14.0
$eeMJ$	0	0.79 ± 0.22
$e\mu MJ$	0	0.96 ± 0.26
νeMJ	0	1.7 ± 0.5
νMJ	36	36.8 ± 6.0
$\nu\mu MJ$	0	0.65 ± 0.25

H1 preliminary e^-p

Channel	data	SM prediction
eLQ	225	223.1 ± 16.2
νLQ	267	274.7 ± 21.5
e^-MJ	28	21.3 ± 3.4
e^+MJ	0	0.11 ± 0.03
$eeMJ$	0	0.29 ± 0.15
$e\mu MJ$	0	0.18 ± 0.04
νeMJ	0	0.43 ± 0.24
νMJ	14	12.2 ± 2.0
$\nu\mu MJ$	0	0.16 ± 0.04

Table 3: Summary of total event numbers for the squark decay channels considered in e^+p collisions (left) and in e^-p collisions (right).

- An mass dependent optimized lower y_e-cut is applied in order to discriminate the SUSY signal from the NC DIS background.
- In addition the selection is restricted to the kinematic range $Q_e^2 > 2500\,\mathrm{GeV}^2$ and $y_e < 0.9$. Excluding the high y values avoids the region where migration effects due to QED radiation in the initial state are largest for the kinematic reconstruction method using the electron. Furthermore background from photoproduction where a jet is misidentified as an electron is suppressed.

The M_e spectra for data and SM background after this selection are shown in figure 1 (top) for e^+p collisions and in figure 2 (top) for e^-p collisions. 690 events are found in the e^+p data set, while 705.9 ± 51.3 are expected from SM processes. In the e^-p data 225 are seen, while 223.1 ± 16.2 is the SM prediction. No significant deviation from SM expectation has been found. The systematic uncertainties of the SM expectation that are taken into account are discussed in section 6.

Squarks undergoing a $\boldsymbol{\nu LQ}$ decay lead to CC DIS-like events with high missing transverse momentum. The events are clustered in the M_h distribution with a resolution of 10 to $20\,\mathrm{GeV}$ depending on the squark mass. The selection criteria for the $\boldsymbol{\nu LQ}$ channel are the following: The missing transverse momentum must be greater than $30\,\mathrm{GeV}$ and no electron/positron must be found with $p_{T,e} > 5\,\mathrm{GeV}$. Again the comparison with SM expectation is restricted to the kinematic range $Q_h^2 > 2500\,\mathrm{GeV}^2$ and $y_h < 0.9$. As mentioned above only $\tilde{d}_R^k$ produced mainly in e^-p collisions can undergo a $\boldsymbol{\nu LQ}$ decay. In this data set we find 267 events and 274.7 ± 21.5 are expected from the SM. The M_h spectra for data and SM background are shown in figure 2 (middle top). No significant deviation from SM expectation has been found.

5.2 Squark Gauge decays leading to e+jets+ X final states

For the channels $\boldsymbol{e^+MJ}$, $\boldsymbol{e^-MJ}$, $\boldsymbol{e\nu MJ}$, $\boldsymbol{e\mu MJ}$ and $\boldsymbol{eeMJ}$ a common preselection has been performed:

- At least one electron (or positron) must be found with $p_{T,e} > 6\,\mathrm{GeV}$ and in the angular range $5^\circ < \theta_e < 110^\circ$. For central electrons/positrons ($\theta_e > 32^\circ$) a charged track in the central tracking system must be associated with the electromagnetic cluster fulfilling matching criteria of cluster and track energy measurement. To discriminate against hadronic photoproduction background faking electrons/positrons in the forward region ($\theta_e < 32^\circ$) electrons/positrons candidates in this region have to fulfill harsher isolation criteria and the $\sum E - p_z$ of the event must be greater than $30\,\mathrm{GeV}$.
- At least two jets must be found with $7^\circ < \theta_{\mathrm{jet}} < 145^\circ$ and $p_{T,\mathrm{jet}} > 15\,\mathrm{GeV}$.
- The minimum of the polar angles of the highest p_T electron/positron and of the two highest p_T jets must fulfill $\mathrm{Min}(\theta_{\mathrm{e}}, \theta_{\mathrm{jet}\,1}, \theta_{\mathrm{jet}\,2}) < 40^\circ$.
- $y_e > 0.4$.
- Of the two highest p_T jets, the one with the larger polar angle θ_{backw}, must satisfy $(y_e - 0.3) > (\theta_{\mathrm{backw}}/\pi)$

The last three cuts exploit the fact that the decay products in squark decays are mainly emitted in the forward direction [1].

After this preselection further cuts are applied for the channels $\boldsymbol{e^+MJ}$ and $\boldsymbol{e^-MJ}$: We ask for balanced events: $p_{T,\mathrm{miss}} < 20\,\mathrm{GeV}$ and $40 < \sum(E - p_z) < 70\,\mathrm{GeV}$. Events are accepted in the channel having the 'wrong' charge lepton (i.e. $\boldsymbol{e^+MJ}$ for e^-p collision and $\boldsymbol{e^-MJ}$ for e^+p collision) if the electron/positron was found in the angular range $\theta_e > 32^\circ$ (where the charge measurement is done with the central tracking system) and the charge was measured accordingly with a significance greater than two standard deviations. The SM expectation in this channel is very low. Table 3 (left) and (right) give the total event numbers for this 'wrong' charge channel for e^+p and e^-p collisions. The data are in agreement with the SM. Electrons or positrons with a charge measurement in the CJC that has the 'right' charge with respect to the initial beam or which are found in the forward region ($\theta_e < 32^\circ$) are accepted in the 'right' charge lepton channel (i.e. $\boldsymbol{e^-MJ}$ for e^-p collision and $\boldsymbol{e^+MJ}$ for e^+p collision). For events in this channel a mass M_{inv} is calculated as: $M_{\mathrm{inv}} = \sqrt{4E_e^0\left(\sum_i E_i - E_e^0\right)}$ where the sum runs over all jets found in the event with $p_{T,\mathrm{jet}} > 5\,\mathrm{GeV}$ and all electrons (or positrons). This reconstruction method yields a typical resolution of 7 to $10\,\mathrm{GeV}$ depending on the squark mass. The M_{inv} distribution for data and SM expectation of the 'right' charge channels $\boldsymbol{eMJ}$ are shown in figure 1 (middle) for e^+p and in figure 2 (middle bottom) for e^-p collisions respectively. No significant deviation from the SM has been observed.

The further selection for the channels $\boldsymbol{elMJ}$ requires an additional electron/positron with the same criteria as described above or an additional muon with $p_{T,\mu} > 5\,\mathrm{GeV}$ in the polar angular range $10^\circ < \theta_\mu < 110^\circ$. In these channels the SM background (mainly NC DIS) is very low. The total event numbers for the $\boldsymbol{eeMJ}$ and $\boldsymbol{e\mu MJ}$ channel are given in table 3 (left) and (right) for e^+p and e^-p collisions respectively. Data and SM expectation are in agreement.

For the channel $\boldsymbol{e\nu MJ}$, after the preselection, $p_{T,\mathrm{miss}} > 15\,\mathrm{GeV}$ is required. The cut $y_e(y_e - y_h) > 0.05$ exploits the fact that, for events coming from a squark decaying into the $\boldsymbol{e\nu MJ}$ channel the escaping neutrino carries a non-negligible part of $\sum(E - p_z)$ and hence the variable y_h is substantially smaller than y_e, while $y_e \sim y_h$ is expected for NC DIS events. The total numbers of events which are found in this channel are given in table 3 (left) and (right) and are in agreement with the SM background, where the main source is NC DIS.

5.3 Squark Gauge decays leading to ν+jets+ X final states

The channels $\boldsymbol{\nu MJ}$ and $\boldsymbol{\nu\mu MJ}$ are selected with a common preselection: We ask for missing transverse momentum $p_{T,\text{miss}} > 25\,\text{GeV}$ and at least two jets with $p_{T,\text{jet}} > 15\,\text{GeV}$ in the angular range $7^\circ < \theta < 145^\circ$. No electron must be found in the events.

If no muon was found, the event was counted in the $\boldsymbol{\nu MJ}$ channel and a invariant mass M_{inv} was calculated from p_T and $E - p_z$ conservation assuming that only one neutrino was present in the event. The mass resolution of this method was found to be around $15\,\text{GeV}$. The mass spectra of data and expected SM background are shown in figure 1 (bottom) and 2 (bottom) for e^+p and e^-p collisions respectively. The data are described by the SM prediction.

If in addition an muon with $p_{T,\mu} > 5\,\text{GeV}$ and $10^\circ < \theta_\mu < 110^\circ$ was found, the events are counted in the $\boldsymbol{\nu\mu MJ}$ channel. In table 3 (left) and (right) the number of selected events are shown for the e^+p and e^-p data set. They are compatible with the SM expectation,which is mainly CC DIS.

6 Systematic Uncertainties

The experimental errors on the expectation from SM processes considered are:

- The uncertainty on the electromagnetic energy scale varies from $0.7\,\%$ to $3\,\%$ depending on the calorimeter region.
- The uncertainty on the hadronic energy scale is 2%.
- An error of $1.5\,\%$ is assigned to the measurement of the integrated luminosity.

A theoretical uncertainty of $\pm 7\,\%$ on the DIS expectations is attributed due to the limited knowledge of the proton structure. A model uncertainty of $\pm 15\,\%$ is assigned on the predicted cross-section for multijet final states.

An additional systematic error arises from the theoretical uncertainty on the signal cross-section, originating mainly from uncertainties on the parton densities. This uncertainty is $7\,\%$ for $\tilde{d}_R^k$ squarks in e^-p collisions and varies between $7\,\%$ at low squark masses up to $50\,\%$ around $290\,\text{GeV}$ for $\tilde{u}_L^j$ in e^+p collisions. Moreover, choosing either Q^2 or the square of the transverse momentum of the final state lepton instead of $M_{\tilde{q}}^2$ as the hard scale at which the parton distribution are estimated yields an additional uncertainty of $\pm 7\,\%$ on the signal cross-section. An uncertainty of $10\,\%$ is attributed to the signal detection efficiencies resulting mainly from the interpolation procedure.

7 Exclusion Limits

No significant deviation from SM expectation has been found in the analysis of various R_p-violating and gauge decay channels. These channels are combined separately for e^+p and e^-p collisions to set constraints on R_p violating SUSY models.

For all channels, we use the numbers of observed and expected events and the signal efficiencies for a given squark mass. For the channels $\boldsymbol{eLQ}$, $\boldsymbol{\nu MJ}$ and $\boldsymbol{eMJ}$ with the 'right' charge ($\boldsymbol{e^- MJ}$ for e^-p collisions and $\boldsymbol{e^+ MJ}$ for e^+p collisions) the numbers of observed and expected events are integrated within a mass bin which slides over the accessible mass range. The width of the mass bin is adapted to the expected mass resolution in each channel. For the channels $\boldsymbol{eMJ}$ with 'wrong' charge, $\boldsymbol{e\ell MJ}$ and $\boldsymbol{\nu\ell MJ}$, where both the SM expectation and the observation are small, no mass restriction is imposed.

The masses of the neutralinos, charginos and gluinos, as well as the couplings between any two SUSY particles and a standard fermion/boson, are determined by the usual MSSM parameters: the "mass" term μ which mixes the Higgs superfields, the SUSY soft-breaking mass parameters M_1, M_2 and M_3 for $U(1)$, $SU(2)$ and $SU(3)$ gauginos, and the ratio $\tan\beta$ of the vacuum expectation values of the two neutral scalar Higgs fields. These parameters are defined at the electroweak scale. We assume that the gaugino mass terms unify at a Grand Unification (GUT) scale to a common value $m_{1/2}$ leading to usual relations [21] between M_1, M_2 and M_3. The masses and decay widths of all involved sparticles have been obtained using the SUSYGEN package.

Assuming a Poisson distribution for the SM background expectations and for the signal, an upper limit on the number of events coming from squark production is obtained using a modified frequentist approach [22]. This limit on the number of events is then translated into an upper bound on the squark cross-section, which in turn leads to constraints on SUSY models. For a fixed set of MSSM parameters and sfermion masses, the branching ratios for the different channels only depend on the Yukawa coupling λ'_{1j1} in e^+p and λ'_{11k} in e^-p collisions. This also holds for the upper limit on the signal cross-section σ_{lim} derived from the combination of the analysed channels. At a given squark mass, Yukawa couplings for which σ_{lim} is smaller than the signal cross-section are excluded. The signal cross-section is obtained from the leading order amplitudes given in [4], corrected by multiplicative K-factors [23] to account for next-to-leading order QCD corrections.

The case of a non-vanishing coupling λ'_{131} for e^+p and λ'_{113} for e^-p allowing for the resonant production of stop and sbottom squarks has to be treated separately since the top and bottom masses can not be neglected in the calculation of the branching ratios. For $\lambda'_{131} \neq 0$ the top quark decays via $t \rightarrow bW$. Most of the stop decays are in fact covered by our analysis, but the efficiencies for the considered channels, which are valid for decay patterns as shown in table 2, can not be used in that case. Conservatively, diagrams which lead to a top in the final state are not taken into account in the calculation of the visible branching ratios.

7.1 Limits in the "phenomenological" MSSM

We consider here a version of the MSSM where the parameters μ, M_2 and $\tan\beta$ are only used to determine the masses and couplings of the gauginos, while the sfermion masses are free parameters. The gluino mass is approximated by the value of M_3 at the electroweak scale. We neglect any possible mixing between sfermions and assume that all squarks are degenerate in mass. Since the limits on λ'_{1j1} and λ'_{11k} are almost independent of the masses of sleptons [1], they are also assumed to be degenerate, and their mass $M_{\tilde{l}}$ is set to a fixed value (90 GeV) close to the lowest mass bound from sfermion searches at LEP.

In order to investigate systematically how the sensitivity depends on the MSSM parameters, a scan of the parameters M_2 and μ is performed, for two values of $\tan\beta = 2$ and 6. The parameters M_2 and μ are varied in the range $70\,\mathrm{GeV} < \mathrm{M}_2 < 350\,\mathrm{GeV}$ and $-300\,\mathrm{GeV} < \mu < 300\,\mathrm{GeV}$. Points which lead to a scalar LSP or to LSP masses below 30 GeV are not considered. This latter restriction, as well as the lower value for M_2, are motivated by the exclusion domains resulting from χ searches in $\not{R}_p$ SUSY at LEP. For each point in this (μ, M_2) plane the upper bound λ'_{lim} on the coupling λ'_{1j1} and λ'_{11k} is obtained. The results for λ'_{1j1} and λ'_{131} are shown in figure 3 for the analysis of the e^+p data. Figure 4 shows the limits on λ'_{11k} $(k = 1, 2)$ and λ'_{113} resulting from the analysis of e^-p. The two full curves in each of these figures indicate the maximal and minimal values obtained for λ'_{lim} within the parameter space investigated. The limits on both λ'_{1j1} and λ'_{11k} are widely independent on the SUSY parameters, as can be seen from the narrow region that is excluded only in part of the parameter space in each plot and from the small differences of the results for $\tan\beta = 2$ and 6. For a Yukawa coupling of electromagnetic strength, (i.e. $\lambda'_{1j1} = 0.3$ or $\lambda'_{11k} = 0.3$) squark masses below $\sim 275\,\mathrm{GeV}$ are excluded at 95% CL. The limits on λ'_{1j1} are valid for $\tilde{u}_L$, $\tilde{c}_L$ and $\tilde{t}_L$, whereas the results on λ'_{11k} are valid for $\tilde{d}_R$, $\tilde{s}_R$ and $\tilde{b}_R$.

Our direct results are compared to indirect limits from low energy experiments [25]. The production of $\tilde{u}$ and $\tilde{d}$ squarks via a λ'_{111} coupling is very severely constrained by neutrinoless double beta decay experiments [24]. The best indirect limit on the coupling λ'_{121} (λ'_{131}), which could allow for the production of squarks $\tilde{c}$ ($\tilde{t}$), comes from atomic parity violation (APV) measurements [25, 26]. The best indirect limit on the coupling λ'_{112} (λ'_{113}), which could allow for the production of squarks $\tilde{s}$ ($\tilde{b}$), results from charge current universality (CCU) [25]. The HERA limits extend the excluded region for squarks of the second and third family (i.e. $\lambda'_{121}, \lambda'_{131}, \lambda'_{112}, \lambda'_{113}$) for masses up to $\sim 240\,\mathrm{GeV}$.

7.2 Limits in the Minimal Supergravity Model

In this section we consider the minimal supergravity (mSUGRA) model [27], where the number of free parameters is reduced by assuming, in addition to the GUT relation between M_1, M_2 and M_3 mentioned in section 7, a universal mass parameter m_0 for all scalar fields at the GUT scale. The evolution of the sfermion masses towards low scales is given by the Renormalisation Group Equations (RGE) and depends on the gauge quantum numbers of the sfermions. As a result, the sfermion masses at the electroweak scale are related to each other and to the parameters determining the gaugino sector. By requiring in addition that the breaking of the electroweak symmetry is driven by radiative corrections (REWSB) the model is completely determined by m_0, $m_{1/2}$, $\tan\beta$, sign of μ and the common trilinear coupling at the GUT scale A_0. The modulus of μ is related to the other model parameters. The program SUSPECT 2.1 [28] is used to obtain the REWSB solution for $|\mu|$ and the full supersymmetric mass spectrum.

Assuming a fixed value for the $R\!\!\!/_p$ coupling λ'_{1j1} or λ'_{11k}, our searches can be expressed in terms of constraints on the mSUGRA parameters, for example on $(m_0, m_{1/2})$ when $\tan\beta$, A_0, and the sign of μ are fixed. A_0 enters only marginally in the interpretation of the results and is set to zero.

Values of the parameters leading to a LSP lighter than $30\,\mathrm{GeV}$ have not been excluded here. However a vanishing efficiency has been assumed for squarks undergoing a gauge decay ending by a χ or $\tilde{g}$ lighter than $30\,\mathrm{GeV}$, since the parametrisation of the efficiencies (see section 4) is not valid in this domain.

7.2.1 Results for the first and second family

For $\mu < 0$, results obtained for a Yukawa coupling $\lambda'_{1j1} = 0.3$ ($j = 1, 2$) are shown in the $(m_0, m_{1/2})$ plane in figure 5 (plots on the left) for three values of $\tan\beta = 2, 6, 10$. The corresponding results for $\lambda'_{11k} = 0.3$ ($k = 1, 2$) derived from e^-p data are shown in figure 6 (plots on the left). The hatched domains correspond to values of the parameters where no REWSB is possible or where the LSP is a sfermion. For $\lambda'_{1j1} = 0.3$ the parameter space where $M_{\tilde{q}} < 275\,\mathrm{GeV}$ is nearly fully excluded. For $\lambda'_{11k} = 0.3$ the squark mass limit is at $280\,\mathrm{GeV}$ because of the higher squark production cross-section in e^-p collisions. At low $m_{1/2}$ values however, where the lightest χ's and the $\tilde{g}$ are lighter than $30\,\mathrm{GeV}$, the sensitivity on the squark mass decreases since the efficiency is conservatively set to zero for all channels but $\boldsymbol{eLQ}$ (and $\boldsymbol{\nu LQ}$). Results of the D0 experiment [29] from searches for R_p violating SUSY which rely on di-electron events are also shown. For $\tan\beta = 2$ the H1 limits are more stringent for low values of m_0, whereas for $\tan\beta = 6$ the excluded domains extend considerably beyond the region ruled out by the D0 experiment. This is due to the fact that, for large values of $\tan\beta$, the lightest neutralino is dominated by its zino component, so that its decay into $e^\pm$ is suppressed. As a result the sensitivity of the di-electron D0 analysis is decreased, while the dominant squark decay mode is still observable in the H1 analysis via the $\boldsymbol{\nu MJ}$ and $\boldsymbol{\nu\ell MJ}$ channels. However, the parameter space is still more constrained by the searches for χ's and sleptons at LEP [5] as shown for $\tan\beta = 2$ in figure 5 (top left) and figure 6 (top left). This is the only value of $\tan\beta$ considered in [5]. But results for $\tan\beta = 6$ and 10 are expected to be similar. LEP and TeVatron limits are independent of the Yukawa coupling.

7.2.2 Results on stop and sbottom production

We now consider a non-vanishing coupling λ'_{131} which could lead to the production of a stop. The weak interaction eigenstates $\tilde{t}_L$ and $\tilde{t}_R$ mix in this case through an angle θ_t to form two mass eigenstates, $\tilde{t}_1 = \cos\theta_t \tilde{t}_L + \sin\theta_t \tilde{t}_R$ and $\tilde{t}_2 = -\sin\theta_t \tilde{t}_L + \cos\theta_t \tilde{t}_R$. The production cross-section of the $\tilde{t}_1$ ($\tilde{t}_2$) scales as $\lambda'^2_{131}\cos^2\theta_t$ ($\lambda'^2_{131}\sin^2\theta_t$). Hence, the lightest stop $\tilde{t}_1$ does not necessarily have the largest production cross-section. Thus both $\tilde{t}_1$ and $\tilde{t}_2$ are searched for in the analysis.

For a non-vanishing λ'_{113} sbottom production could be possible. Similar to the stop states the weak sbottom states ($\tilde{b}_L$, $\tilde{b}_R$) mix to form mass eigenstates, $\tilde{b}_1 = \cos\theta_b \tilde{b}_L + \sin\theta_b \tilde{b}_R$ and $\tilde{b}_2 = -\sin\theta_b \tilde{b}_L + \cos\theta_b \tilde{b}_R$. The production cross-section for $\tilde{b}_1$ ($\tilde{b}_2$) scales as $\lambda'^2_{113}\sin^2\theta_b$

($\lambda'^2_{113}\cos^2\theta_b$). The case of sbottom mixing is treated in the same way as in the stop case. For the latter the procedure is explained in the following.

For the channels $\boldsymbol{eMJ}$ with 'wrong' charge, $\boldsymbol{e\ell MJ}$ and $\boldsymbol{\nu\ell MJ}$, where the signal is integrated over the whole mass range, the fraction of the visible signal in a given channel, k, is $\sum_{i=1,2}\beta_{k,i}\varepsilon_{k,i}\sigma_i/\sigma_{tot}$, where $\beta_{k,i}$ is the branching ratio for $\tilde{t}_i$ to decay into this channel k, $\varepsilon_{k,i}$ is the corresponding selection efficiency, σ_i is the production cross-section of $\tilde{t}_i$, and $\sigma_{tot}=\sigma_1+\sigma_2$ is the total signal cross-section. For the channels $\boldsymbol{eLQ}$,$\boldsymbol{\nu LQ}$, $\boldsymbol{eMJ}$ with 'right' charge and $\boldsymbol{\nu MJ}$ where the signal is integrated over a "sliding mass bin" only the contribution of the state $\tilde{t}_i$ for which the sensitivity is maximal (i.e. which maximises $\sigma_i(\sum_k\beta_{k,i}\varepsilon_{k,i})$) is taken into account in the above summation. The numbers of observed and expected events are then integrated in the mass bin corresponding to $\tilde{t}_i$ only.

Using this procedure exclusion limits have been derived for $A_0=0$, $\mu<0$ and $\tan\beta=2,6$ and 10. The excluded regions in the $(m_0,m_{1/2})$ plane for $\lambda'_{131}=0.3$ (stop) and $\lambda'_{113}=0.3$ (sbottom) are shown in figure 5 (plots on the right) and figure 6 (plots on the right) respectively. The domain below the line $m_{1/2}\lesssim 10\,\mathrm{GeV}$ is not considered since it corresponds to cases where the only allowed LSP decay into $\nu b\bar{d}$ is kinematically forbidden.

In case of stop production (figure 5, plots on the right) for $\tan\beta=2$, the excluded domain is slightly larger than that ruled out previously for $\lambda'_{1j1}=0.3$ ($j=1,2$) due to the mixing in the stop sector which leads to $\tilde{t}_1$ masses smaller than the masses of the other $\tilde{u}^j_L$ squarks. In particular, larger values of m_0 can be probed. This remains the case for $\tan\beta=6$ and 10 as long as $m_{1/2}$ is large enough to ensure that the mass of the lightest neutralino is above $30\,\mathrm{GeV}$. When the χ^0_1 becomes too light, the efficiencies for the channels involving a $\chi^+_1\rightarrow\chi^0_1$ decay are set to zero, and the sensitivity to the signal is only provided by the $\boldsymbol{eLQ}$ channel or by the decays $\tilde{t}\rightarrow b\chi^+_1$ followed by a $\not{R}_p$ decay of the chargino. As a result, only lighter stops can be probed, for which the visible cross-section is large enough. Note that for $\tan\beta=2$ $(6,10)$, $\tilde{t}_1$ masses up to $265\,\mathrm{GeV}$ ($270\,\mathrm{GeV}$) can be excluded for $\lambda'_{131}=0.3$. These masses are smaller than the maximal sensitivity reached, for the same coupling value for $j=1,2$ because of the $\cos^2\theta_t$ reduction of the $\tilde{t}_1$ cross-section. For $\tan\beta=2$ the limits obtained by this analysis are comparable to the L3 sensitivity in χ and slepton searches at intermediate values of m_0. In the same part of the parameter space, the H1 limits extends considerably beyond the expected LEP sensitivity for higher values of $\tan\beta$.

In the case of sbottom production (figure 6, plots on the right) the limits are very similiar to those obtained for $k=1,2$, since the mixing in the sbottom sector is small. The sensitivity follows curves of equal $\tilde{b}_2$ masses because the production cross-section for this state is much higher than for $\tilde{b}_1$ if the mixing angle is small. $\tilde{b}_2$ masses up to $280\,\mathrm{GeV}$ are ruled out.

7.2.3 Dependence of the results on $\tan\beta$

In order to check the dependence of our results on $\tan\beta$, a scan of this parameter has been performed. The number of free parameters has been reduced by setting the masses m_0 and $m_{1/2}$ to a common value M. The limits on M are shown in figure 7 as a function of $\tan\beta$ for $\lambda'_{1jk}=0.3$. All squark flavours are considered. The exclusion curves are rather flat for the first two families since mixing effects are very small. Assuming equal $\not{R}_p$ couplings a larger part of the parameter space is excluded for $\tilde{d}$ and $\tilde{s}$ production (shown in blue) as for $\tilde{u}$ and $\tilde{c}$ production (darkred) because of the higher squark production cross-section in e^-p collisions. For squarks of the third family mixing effects get important. With higher values of $\tan\beta$ the increase of the mixing angle θ_b results in an improvement of the sbottom limit (shown in red) since it leads to a smaller $\tilde{b}_1$ mass giving a higher $\tilde{b}_1$ production cross-section. The mixing effects are largest in the stop sector leading to very stringent limits on M (shown in green). For low values of $\tan\beta$ the $\cos^2\theta_t$ reduction of the $\tilde{t}_1$ production cross-section is important. For values of $\tan\beta \gtrsim 39$ the mixing of the two stau ($\tilde{\tau}$) states leads to decay chains involving staus which result in final states including τ leptons. These channels are not searched for explicitly. Thus in this corner of the parameter space the limit on stop production gets weaker.

8 Conclusion

We have searched for squarks in e^+p and e^-p collisions at HERA in R-parity violating SUSY models. No evidence for the resonant production of $\tilde{u}$, $\tilde{c}$, $\tilde{t}$, $\tilde{d}$, $\tilde{s}$ and $\tilde{b}$ was found in the various channels considered which cover almost all decay modes. Mass dependent limits on R-parity violating couplings were derived. The limits were set within the phenomenological MSSM and the minimal Supergravity model. The model dependence of the results was studied in detail by performing a scan of the MSSM parameters and was found to be small.

In the large part of the MSSM parameter space covered by the scan, the existence of squarks of all flavours with masses up to $275\,\mathrm{GeV}$ is excluded at 95% confidence level for a strength of the Yukawa coupling equal to α_{em}. This mass limit extends considerable beyond the limits set by other collider experiments. For lower values of λ' the results improve the indirect bounds set by low-energy experiments. In models where the sfermion masses depend on the parameters which determine the supersymmetric gauge sector, the limits extend beyond the constraints obtained at the TeVatron and LEP collider in part of the parameter space for a Yukawa coupling of electromagnetic strength.

References

[1] C. Adloff *et al.* [H1 Collaboration], Eur. Phys. J. **C20** (2001) 639 [hep-ex/0007035].

[2] T. Ahmed *et al.* [H1 Collaboration], Z. Phys. **C64** (1994) 545.

[3] J. Butterworth and H. Dreiner, Nucl. Phys. **B397** (1993) 3 [hep-ph/9211204] and references therein.

[4] W. Buchmüller, R. Rückl and D. Wyler, Phys. Lett. **B191** (1987) 442 and *Erratum* Phys. Lett. **B448** (1999) 320.

[5] M. Acciarri *et al.* [L3 Collaboration], Eur. Phys. J. **C19** (2001) 397 [hep-ex/0011087].

[6] I. Abt *et al.* [H1 Collaboration], Nucl. Instrum. Meth. **A386** (1997) 310.

[7] B. Andrieu *et al.* [H1 Calorimeter Group], Nucl. Instrum. Meth. **A336** (1993) 460.

[8] B. Andrieu *et al.* [H1 Calorimeter Group], Nucl. Instrum. Meth. **A350** (1994) 57;
B. Andrieu *et al.* [H1 Calorimeter Group], Nucl. Instrum. Meth. **A336** (1993) 499.

[9] DJANGO 6.2; G.A. Schuler and H. Spiesberger, Proc. of the Workshop Physics at HERA, W. Buchmüller and G. Ingelman (Editors), (October 1991, DESY-Hamburg) Vol. 3 p. 1419.

[10] L. Lönnblad, Comput. Phys. Commun. **71** (1992) 15.

[11] G. Gustafson and U. Pettersson, Nucl. Phys. **B306** (1988) 746;
idem, *addendum* Lund University preprint LU-TP-87-19, (October 1987) 4pp.;
B. Andersson, G. Gustafson, L. Lönnblad and U. Pettersson, Z. Phys. **C43** (1989) 625.

[12] H. Jung, Comput. Phys. Commun. **86** (1995) 147.

[13] V. N. Gribov and L. N. Lipatov, Sov. J. Nucl. Phys. **15** (1972) 438;
G. Altarelli and G. Parisi, Nucl. Phys. **B126** (1977) 298;
Y. L. Dokshitzer, Sov. Phys. JETP**46** (1977) 641.

[14] C. Adloff *et al.* [H1 Collaboration], Eur. Phys. J. **C17** (2000) 567 [hep-ex/0007035].

[15] H.-L. Lai *et al.* Eur. Phys. J. **C12** (2000) 375 [hep-ph/0201195].

[16] T. Sjöstrand, Lund Univ. preprint LU-TP-95-20 (August 1995) 321pp;
idem, CERN TH-7112 (1993) [hep-ph/9508391].

[17] PYTHIA 5.7; T. Sjöstrand, CERN-TH-6488 (1992);
T. Sjöstrand, Comput. Phys. Commun. **82** (1994) 74.

[18] U. Baur, J. A. Vermaseren and D. Zeppenfeld Nucl. Phys. Commun. **B375** (1992) 3.

[19] LEGO 0.02; K. Rosenbauer, PhD. thesis, RWTH Aachen (in German), PITHA 95/16 (July 1995).

[20] S. Katsanevas and P. Morawitz, Comput. Phys. Commun. **112** (1998) 227 [hep-ph/9711417];
N. Ghodbane, S. Katsanevas, P. Morawitz, E. Perez, SUSYGEN 3, [hep-ph/9909499].

[21] H. P. Nilles, Phys. Rept. **110** (1984) 1;
H. E. Haber and G. L. Kane, Phys. Rept. **117** (1985) 75.

[22] T. Junk, Nucl. Instrum. Meth. **A434** (1999) 435.

[23] T. Plehn, H. Spiesberger, M. Spira and P. M. Zerwas, Z. Phys. **C74** (1997) 611 [hep-ph/9703433].

[24] R. N. Mohapatra, Phys. Rev. D **34** (1986) 3457;
J. D. Vergados, Phys. Lett. **B184** (1987) 55;
M. Hirsch, H. V. Klapdor-Kleingrothaus and S. G. Kovalenko, Phys. Lett. **B352** (1995) 1 [hep-ph/9502315];
M. Hirsch, H. V. Klapdor-Kleingrothaus and S. G. Kovalenko, Phys. Rev. Lett. **75** (1995) 17;
M. Hirsch, H. V. Klapdor-Kleingrothaus and S. G. Kovalenko, Phys. Rev. D **53** (1996) 1329 [hep-ph/9502385].

[25] H. Dreiner, published in “Perspectives on Supersymmetry” (1997), Ed. G.L. Kane, World Scientific, p 462 [hep-ph/9707435].

[26] P. Langacker, Phys. Lett. **B256** (1991) 277.

[27] M. Drees and M. M. Nojiri, Nucl. Phys. **B369** (1992) 54;
H. Baer and X. Tata, Phys. Rev. D **47** (1993) 2739;
G. L. Kane, C. Kolda, L. Roszkowski and J. D. Wells, Phys. Rev. D **49** (1994) 6173 [hep-ph/9312272].

[28] SUSPECT 2.1, code written by A. Djouadi, J.L. Kneur and G. Moultaka.

[29] B. Abbott *et al.* [D0 Collaboration], Phys. Rev. Lett. **83** (1999) 4476 [hep-ex/9907019].

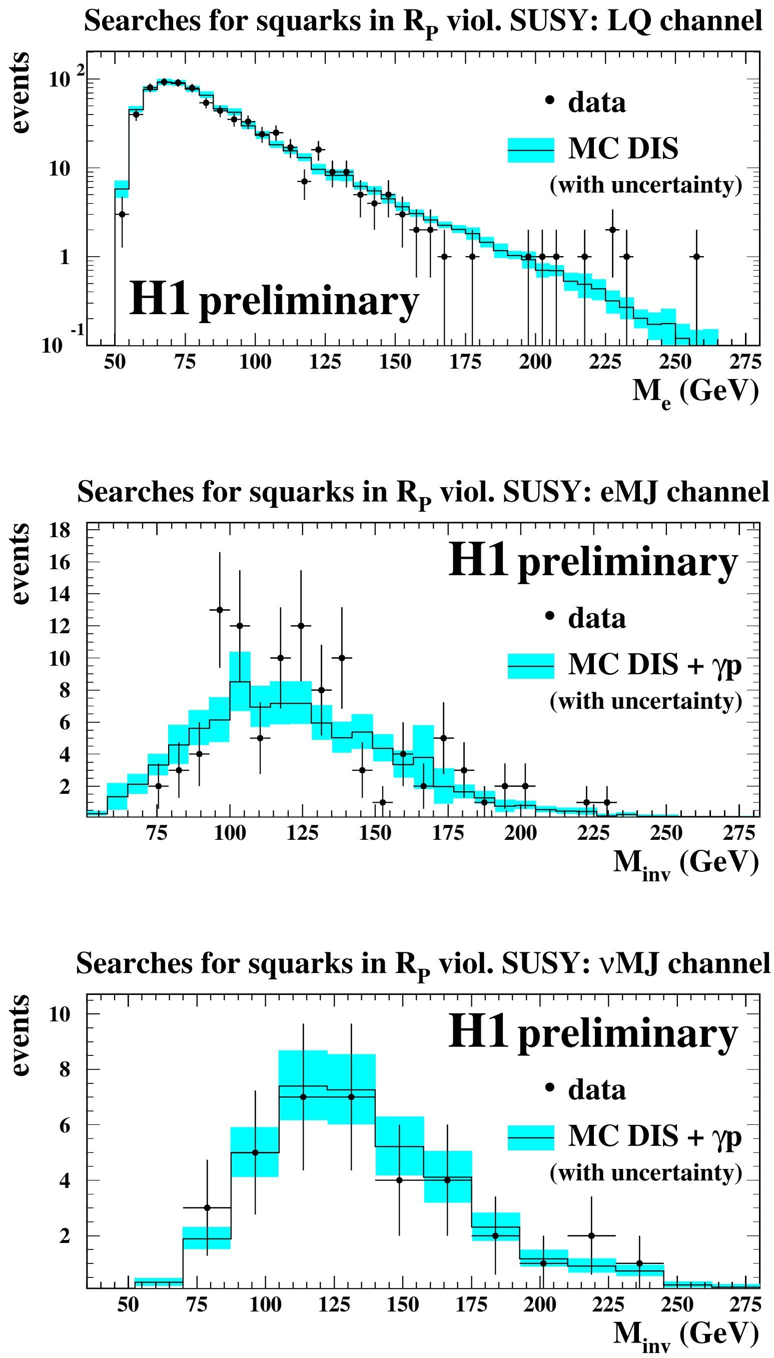

Figure 1: Mass spectra in e^+p collisions: (top): eLQ channel. (middle): eMJ channel with 'right' charge. (bottom): νMJ channel .

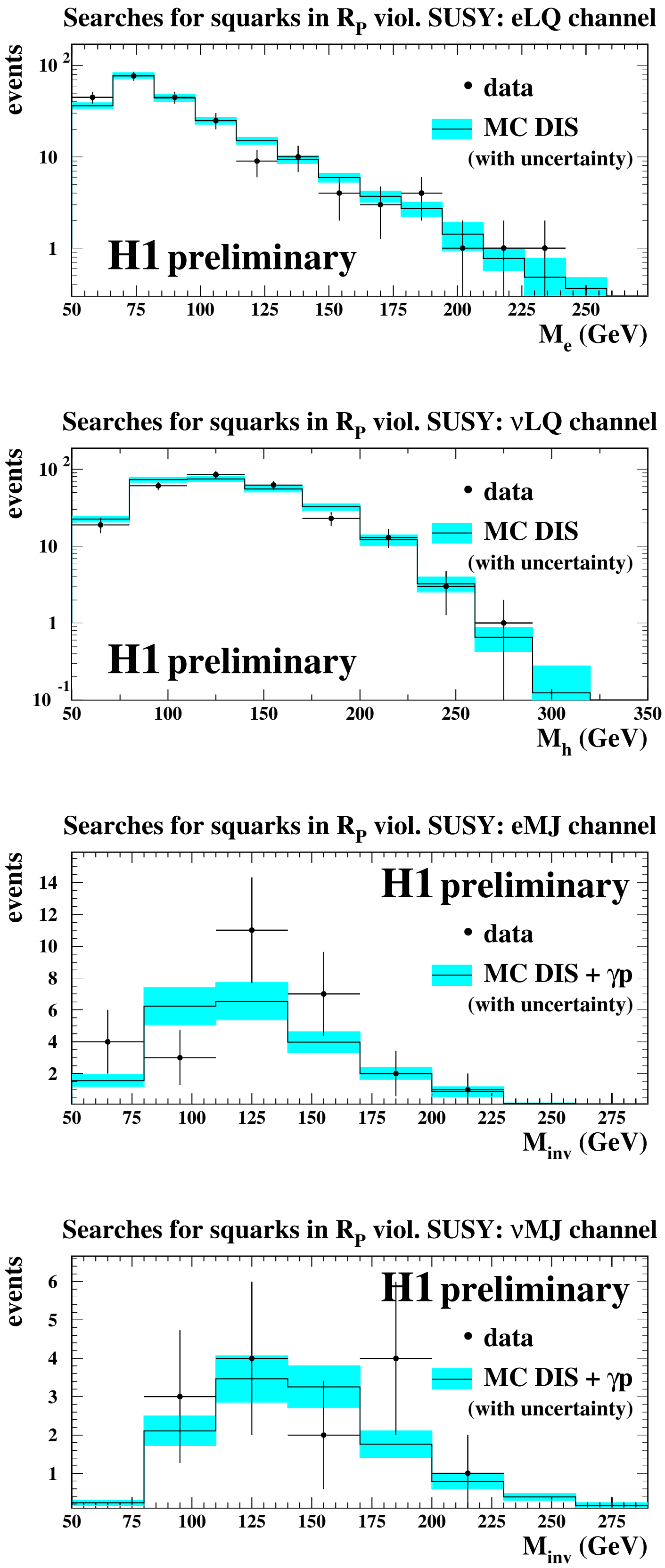

Figure 2: Mass spectra in e^-p collisions: (top): $\boldsymbol{eLQ}$ channel. (middle top): $\boldsymbol{\nu LQ}$ channel. (middle bottom): $\boldsymbol{eMJ}$ channel with 'right' charge. (bottom): $\boldsymbol{\nu MJ}$ channel.

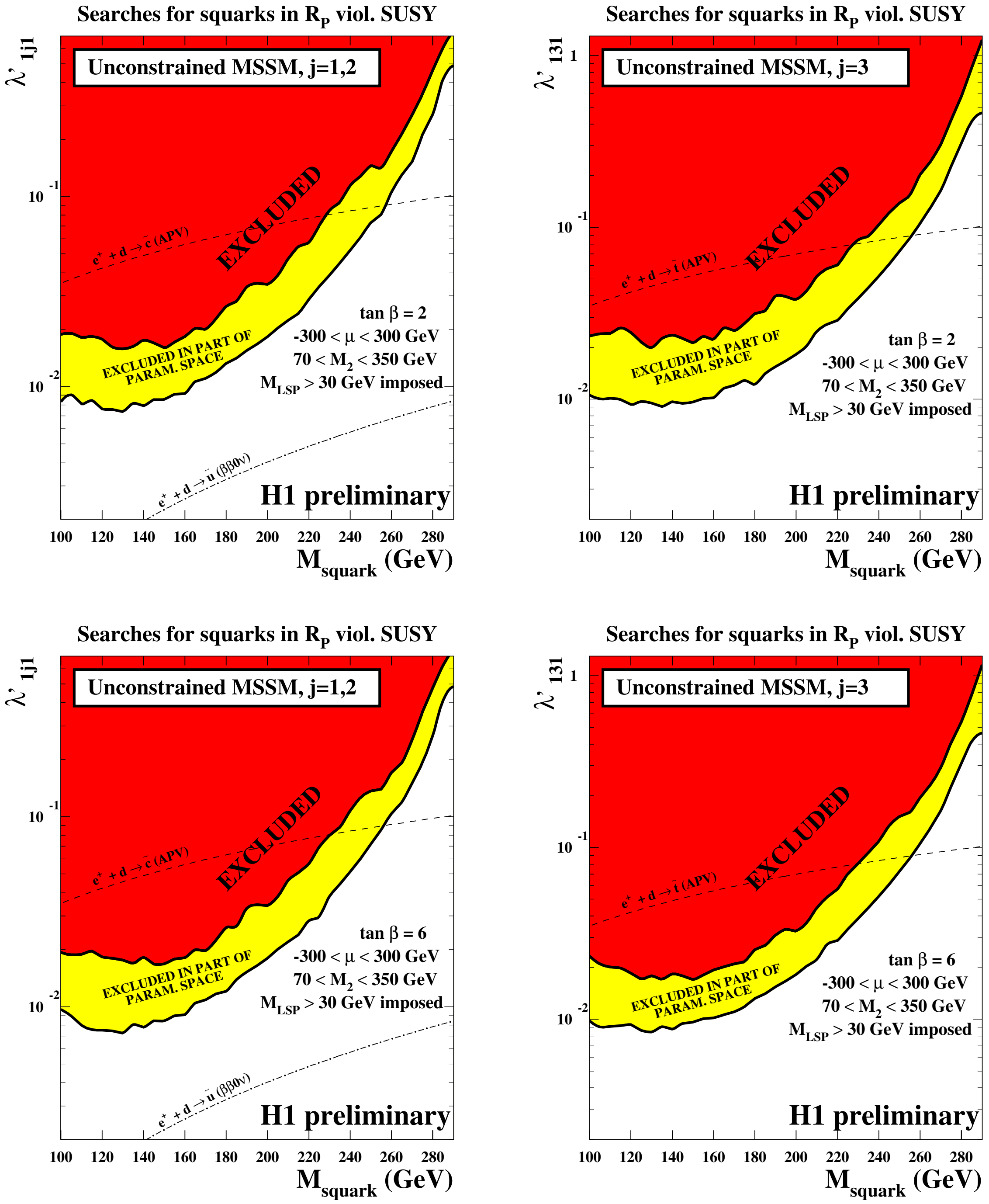

Figure 3: Limits on λ'_{1j1} for $j = 1, 2$ (left) and $j = 3$ (right) as a function of squark mass from a scan in SUSY parameter space for $\tan\beta = 2$ (upper plots) and for $\tan\beta = 6$ (bottom plots). Shown is the strongest (yellow, grey) and the weakest (red, dark) value for the coupling limit. The limits are derived from an analysis of e^+p collisions and are valid for $\tilde{u}^j_L$ squarks (i.e. $\tilde{u}_L$, $\tilde{c}_L$ and $\tilde{t}_L$). Squarks are assumed to be degenerate in mass.

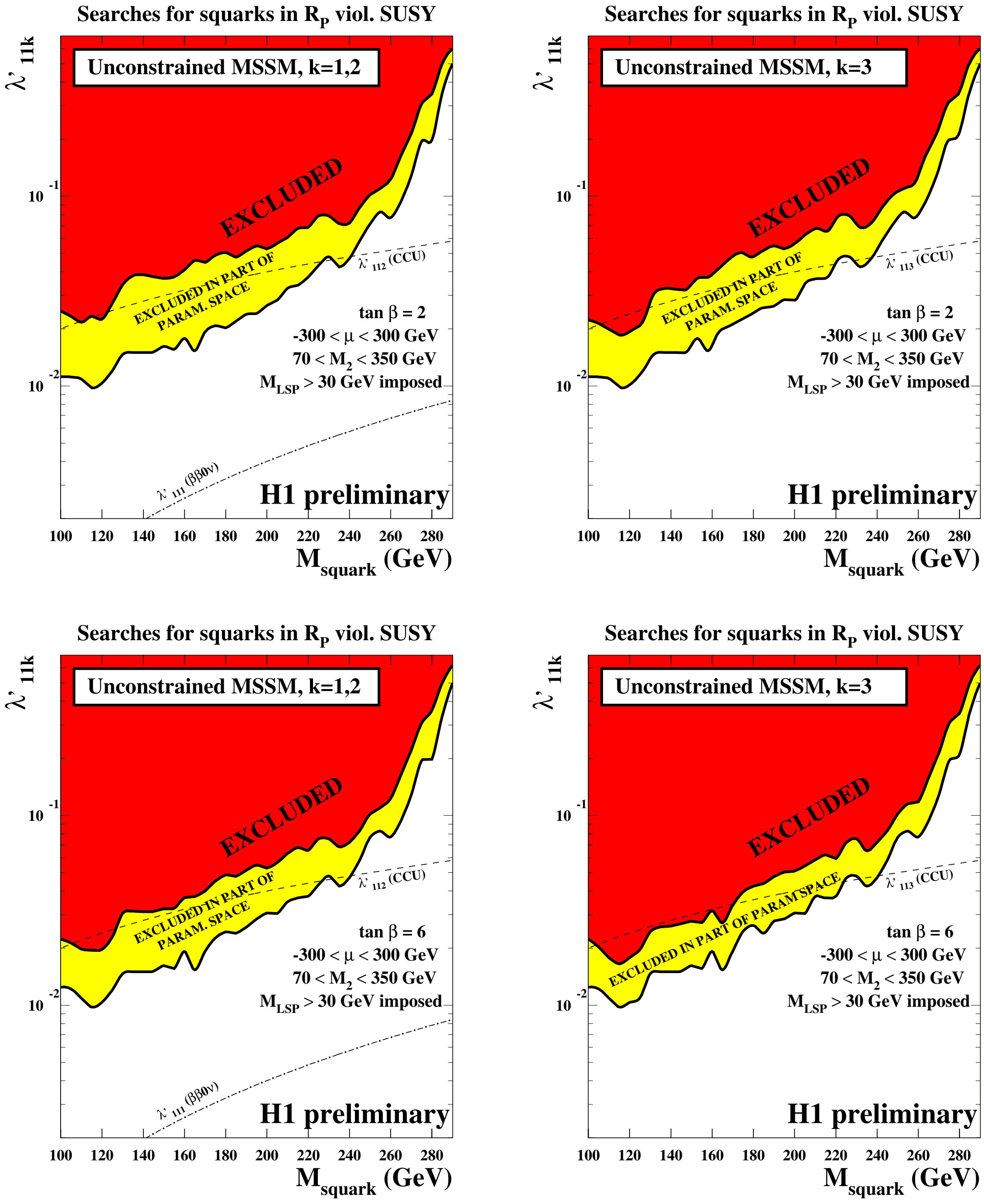

Figure 4: Limits on λ'_{11k} for $k = 1, 2$ (left) and $k = 3$ (right) as a function of squark mass from a scan in SUSY parameter space for $\tan\beta = 2$ (upper plots) and for $\tan\beta = 6$ (bottom plots). Shown is the strongest (yellow, grey) and the weakest (red, dark) value for the coupling limit. The limits are derived from an analysis of e^-p collisions and are valid for $\tilde{d}^k_R$ squarks (i.e. $\tilde{d}_R$, $\tilde{s}_R$ and $\tilde{b}_R$). Squarks are assumed to be degenerate in mass.

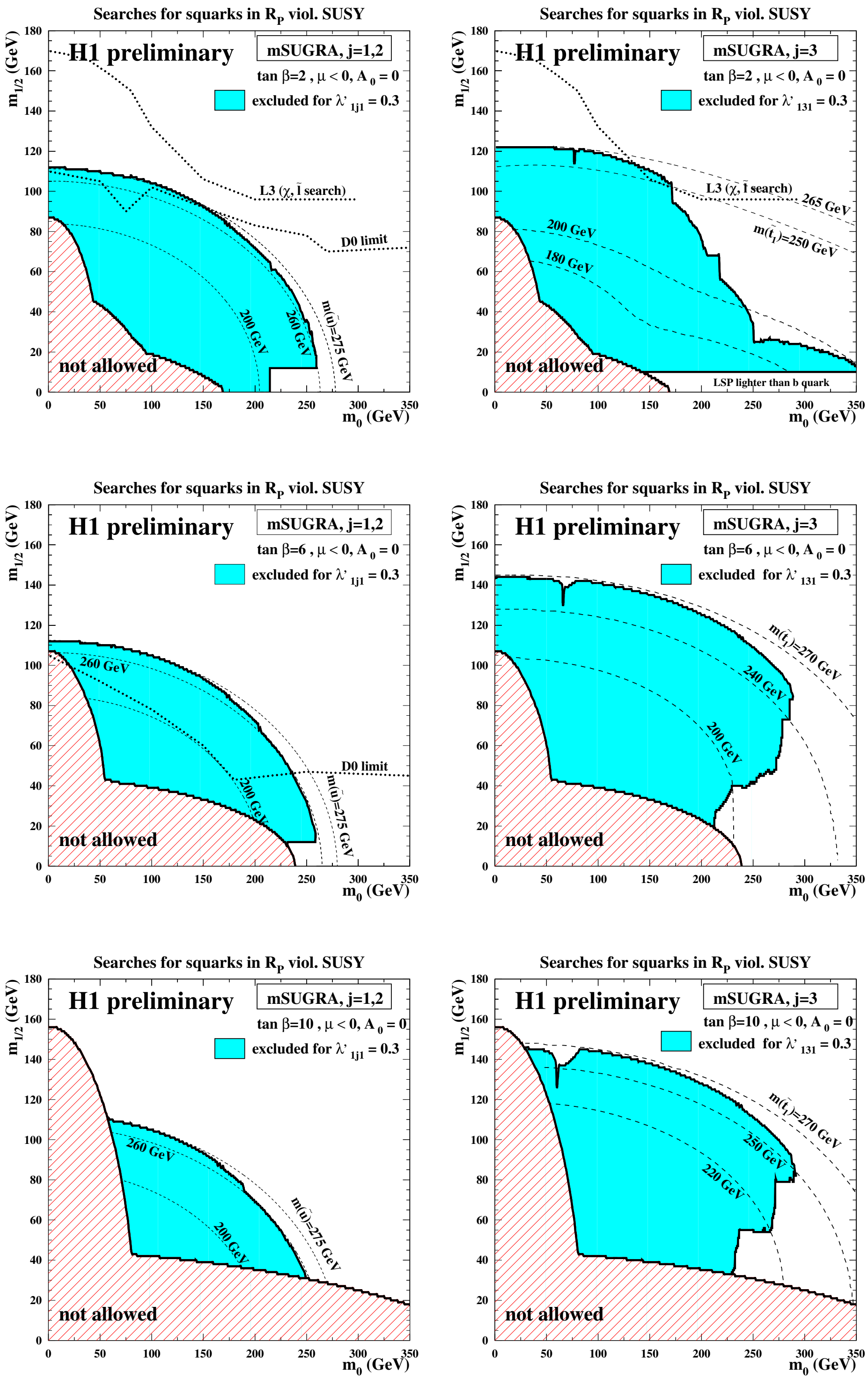

Figure 5: Limits in the minimal Super–Gravity model with $\tan\beta = 2, 6$ and 10 for $\lambda'_{1j1} = 0.3$ with $j = 1, 2$ (plots on the left), i.e. $\tilde{u}$ and $\tilde{c}$ production, and for $\lambda'_{131} = 0.3$ (plots on the right), i.e. $\tilde{t}$ production. Shown are the area that is not allowed in the model (hatched) and the area that is excluded by H1. Curves of constant squark masses are also shown. In case of $\tilde{t}$ production ($j = 3$, right side) the mixing of the stop states is taken into account and curves of constant $\tilde{t}_1$ mass are shown. The regions below the dotted curves are excluded by D0 and L3 respectively.

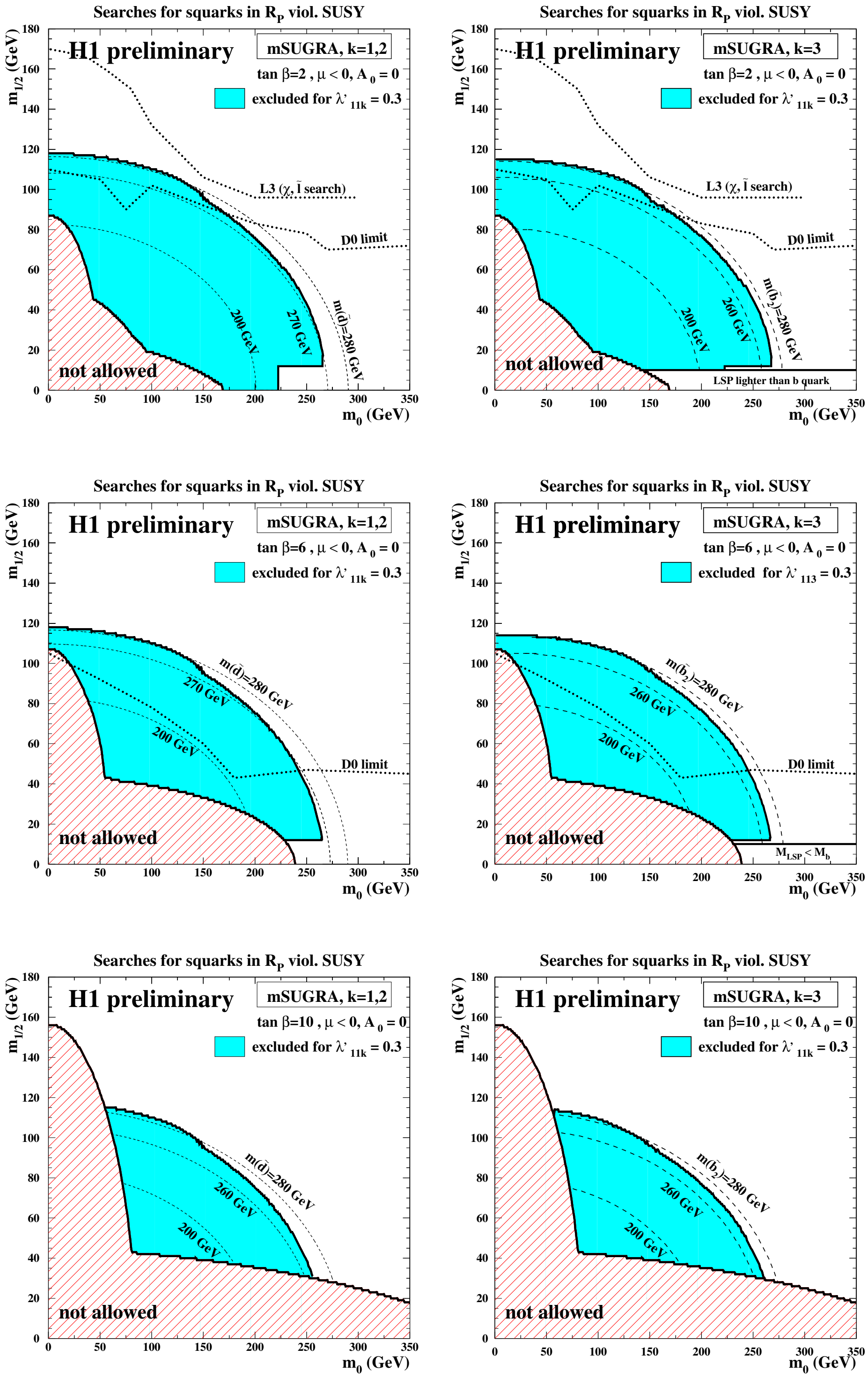

Figure 6: Limits in the minimal Super–Gravity model with $\tan\beta = 2, 6$ and 10 for $\lambda'_{11k} = 0.3$ with $k = 1, 2$ (plots on the left), i.e. $\tilde{d}$ and $\tilde{s}$ production, and for $\lambda'_{113} = 0.3$ (plots on the right), i.e. $\tilde{b}$ production. Shown are the area that is not allowed in the model (hatched) and the area that is excluded by H1 (blue). Curves of constant squark masses are also shown. In case of $\tilde{b}$ production ($k = 3$, right side) the mixing of the sbottom states is taken into account and curves of constant $\tilde{b}_2$ mass are shown. The regions below the dotted curves are excluded by D0 and L3 respectively.

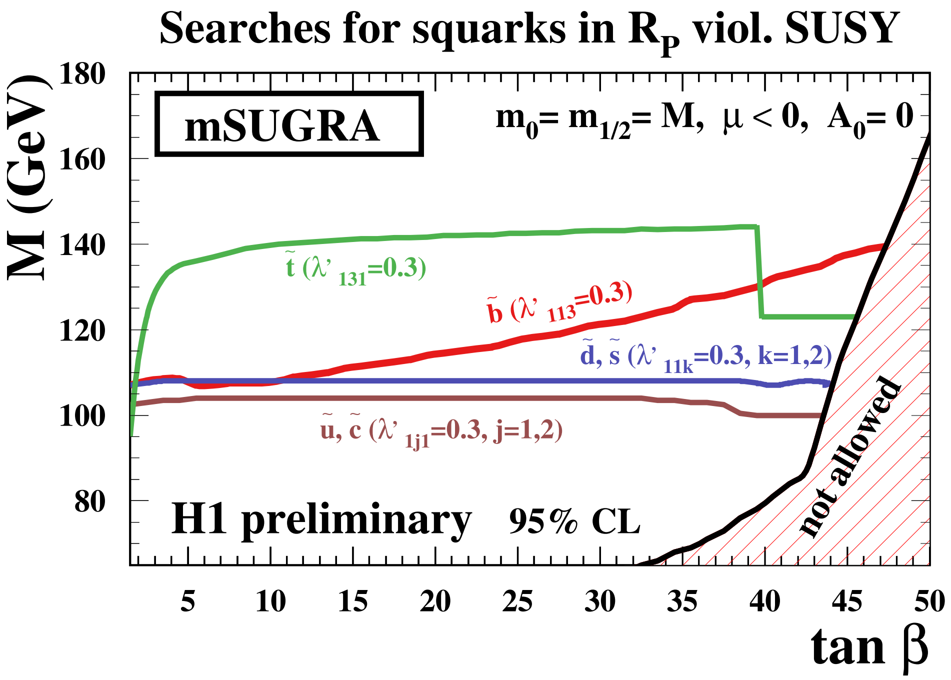

Figure 7: Limits on $m_0 = m_{1/2} = M$ in the minimal Super–Gravity model as a fuction of $\tan\beta$. All squark flavours are considered. Shown are the 95 % exclusion limits for $\lambda'_{1jk} = 0.3$. The areas below the curves are excluded.